Preprints of the 21st IFAC World Congress (Virtual)
Berlin, Germany, July 12-17, 2020

Improving Wafer Stage Performance With Multiple Hybrid Integrator-Gain Systems

Sebastiaan van den Eijnden * **Michiel Francke** **
Henk Nijmeijer * **Marcel Heertjes** *,**

* *Mechanical Engineering Department, Eindhoven, University of Technology, The Netherlands (e-mail: s.j.a.m.v.d.eijnden@tue.nl).*
** *Mechatronic System Design Department, ASML, The Netherlands*

Abstract: An experimental demonstration is given of a nonlinear feedback controller applied to a short-stroke wafer stage system of an industrial wafer scanner. The controller design adopts a classical linear PID-based configuration in which both the integrator and low-pass filter are replaced with hybrid integrator-gain-based filter elements. The reduced phase lag associated with these filters gives rise to increased design flexibility, and potentially enables a substantial increase in low-frequency disturbance suppression. The nonlinear controller is designed by means of a quasi-linear loop-shaping approach, while stability of the full nonlinear closed-loop system is verified by solving a set of linear matrix inequalities. Performance of the controlled system is discussed on the basis of measurement results obtained from a wafer stage system.

Keywords: Motion control, hybrid integrator-gain system, describing function, wafer scanner.

1. INTRODUCTION

Wafer scanners arguably employ one of the crucial steps in the manufacturing process of integrated circuits (IC's), namely, exposing the circuit topology obtained from a reticle onto the photosensitive layers of a silicon wafer. Both reticle and wafer are part of separate motion systems: the reticle stage and wafer stage (Butler, 2011). Essential for these stages to achieve nanometer positioning accuracies while being subject to large acceleration profiles, is the use of feedforward and feedback control systems. While feedforward control is applied for set-point tracking, feedback control typically deals with disturbances. Currently, the majority of feedback control designs rely on the linear control paradigm. The widespread use of linear control in industry is often attributed to its design simplicity and predictability. However, in view of the growing performance demands on accuracy and throughput of wafer scanners, classical trade-offs encountered when using linear control increasingly become performance-limiting factors (Seron et al., 1997). Nonlinear control strategies deal with such trade-offs in a different manner and may offer a means to enhance performance beyond the capabilities of linear control. Examples in this regard include split-path nonlinear (SPAN) filters (Foster et al., 1966), reset control (Beker et al., 2004; Nešić et al., 2008), and hybrid integrator-gain systems (HIGS) (Heertjes et al., 2018).

In the context of high-precision motion control of wafer scanners, HIGS is of particular interest as its describing function reveals (weak) integrator characteristics with an induced phase lag of only 38.15 degrees. This significant phase reduction may be exploited in a control design to enhance frequency-domain characteristics such as bandwidth, thereby giving rise to improved low-frequency disturbance suppression properties. Although a similar phase advantage is associated with reset integrators, HIGS attains its desirable properties by means of continuous (but non-smooth) outputs, whereas reset elements achieve this by discontinuous outputs. Since wafer and reticle stages typically have structural dynamics with lightly damped resonances (Oomen et al., 2014), avoiding discontinuous signals provides a distinct advantage over reset control.

Recently in Van den Eijnden et al. (2020), the phase advantages associated with HIGS are exploited in a PID-based controller design for a motor-load motion system. In particular, a classical PID configuration is considered in which the integrator and second-order low-pass filter are replaced by HIGS-equivalent filters. The latter are constructed by augmenting the HIGS with specific linear input- and output weighting filters, such that the describing function of the augmented HIGS filter demonstrates similar magnitude characteristics as the linear filter it is intended to replace, while giving improved phase properties. A comparable idea was proposed in Saikumar et al. (2019) where a reset element was combined with a linear lead filter for the construction of a constant-in-gain lead-in-phase element to be used for broadband phase compensation.

In this paper, application of the proposed control strategy using multiple HIGS elements is considered. The main contribution is the experimental demonstration of a full HIGS-based PID control design on a short-stroke wafer stage of a state-of-the-art industrial wafer scanner. Performance of the HIGS-based controller is compared to that of a linear equivalent design in terms of (low-frequency) disturbance suppression properties and noise response. Both controllers are designed by means of a (quasi-linear) loop-shaping procedure for maximizing the bandwidth while satisfying identical constraints on the closed-loop transfer functions. As a second contribution, rigorous conditions for

⋆ This work is partially supported by ASML.

stability of the resulting nonlinear closed-loop system are given in the form of numerically tractable linear matrix inequalities (LMIs), which for the case of using multiple HIGS elements are presented for the first time.

The remainder of the paper is organized as follows. In Section 2 HIGS is introduced. Its use for wafer stage control is discussed in Section 3. Section 4 presents sufficient conditions for stability. Loopshaping design and measurement results of the full HIGS-based controller applied to an industrial wafer stage system are presented in Section 5. Section 6 gives the main conclusions.

2. HYBRID INTEGRATOR-GAIN SYSTEMS

The hybrid integrator-gain system (HIGS) can be modelled as the following discontinuous piecewise linear system

$$\mathcal{H}: \begin{cases} \dot{x}_h = \omega_h z & \text{if } (z,u,\dot{z}) \in \mathcal{F}_1, \\ \dot{x}_h = k_h \dot{z} & \text{if } (z,u,\dot{z}) \in \mathcal{F}_2, \\ u = x_h, \end{cases} \tag{1}$$

where $x_h \in \mathbb{R}$ denotes the state of the integrator, $z \in \mathbb{R}$ is the input which is assumed to be continuously differentiable, $\dot{z} \in \mathbb{R}$ is the corresponding time-derivative, and $u \in \mathbb{R}$ is the generated output. The design parameter $\omega_h \in (0,\infty)$ is the integrator frequency, and $k_h \in (0,\infty)$ the gain. Dictated by the sets $\mathcal{F}_1$ and $\mathcal{F}_2$ in (1), the HIGS operates as (i) an integrator or (ii) a gain, respectively. By design, the union of these sets is given by

$$\mathcal{F} := \mathcal{F}_1 \cup \mathcal{F}_2 = \left\{(z,u,\dot{z}) \in \mathbb{R}^3 \mid k_h z u \geq u^2\right\}, \tag{2}$$

which restricts the input-output relation of the HIGS to the $[0,k_h]$-sector. As the HIGS is intented to primarily exhibit integrator dynamics, the region $\mathcal{F}_1$ is maximized in such a way that a switch from 'integrator-mode' to 'gain-mode' is invoked only when the $(z,u,\dot{z})$-trajectory tends to escape the sector, resulting in:

$$\mathcal{F}_1 := \mathcal{F} \setminus \mathcal{F}_2, \tag{3a}$$

$$\mathcal{F}_2 := \left\{(z,u,\dot{z}) \in \mathcal{F} \mid u = k_h z \wedge \omega_h z^2 > k_h \dot{z} z\right\}. \tag{3b}$$

For ensuring $x_h(t) \in \mathcal{F}$ for all $t \geq 0$, one can initialize [1] the HIGS at $x_h(0) \in \mathcal{F}$.

In frequency-domain, HIGS can be approximated by its first-order describing function $\mathcal{D}(j\omega) \in \mathbb{C}$, *i.e.*, the complex mapping from a sinusoidal input $z(t) = \sin(\omega t)$ to the first harmonic in the resulting output $u(t)$. This mapping is given by

$$\begin{aligned} \mathcal{D}(j\omega) = &\frac{\omega_h}{j\omega}\left(\frac{\gamma}{\pi} + j\frac{e^{-2j\gamma}-1}{2\pi} - 4j\frac{e^{-j\gamma}-1}{2\pi}\right) \\ &+ k_h\left(\frac{\pi-\gamma}{\pi} + j\frac{e^{-2j\gamma}-1}{2\pi}\right), \end{aligned} \tag{4}$$

where $\gamma = 2\arctan(k_h\omega/\omega_h) \in [0,\pi]$ denotes the (periodic) switching instant. The describing function (4) demonstrates first-order low-pass magnitude characteristics, with an induced phase lag of only 38.15 degrees. For a derivation of (4), further motivation for the sets (3), and a thorough discussion on the (time-domain) properties of HIGS, see Heertjes et al. (2018) and the references therein.

[1] For an incorrect initialization, *i.e.*, $x_h(0) \notin \mathcal{F}$, a one-time reset occurrence can be enforced by $x_h(0^+) = \alpha \cdot z(0), \alpha \in [0,k_h]$ to ensure $x_h(t) \in \mathcal{F}$ for all $t > 0$.

3. WAFER STAGE CONTROL WITH HIGS

3.1 Scanning Principle and Motion Control Context

During wafer scanning, light emitted by a source falls on a reticle, which contains the blueprint of the integrated circuit topology. After passing through the reticle, the light travels through a lens which projects an image of the circuit topology onto a silicon wafer. The wafer is carried by a short-stroke stage. For driving the stage, Lorentz actuators are used which guarantee a natural decoupling of base-frame vibrations to the stage (Butler, 2011).

For high-quality imaging, the vertical direction of the wafer during scanning should be kept in focus, *i.e.*, the wafer stage generally tracks a non-zero set-point in this direction, reflecting the measured wafer topology. In z-direction, the short-stroke wafer stage is typically approximated by a simplified fourth-order system

$$P(s) = \frac{m_1 s^2 + bs + k}{m_1 m_2 s^4 + b(m_1+m_2)s^3 + k(m_1+m_2)s^2}, \tag{5}$$

where $m_1 = 5$ kg, $m_2 = 17.5$ kg represent the mass of the magnetic yoke mounted to the stage and the stage itself, respectively, and the stiffness coefficient $k = 7.4 \cdot 10^7$ N/m, and damping coefficient $b = 90$ Ns/m reflect properties of the coupling between the yoke and stage. The frequency response function (FRF) of a short-stroke wafer stage in z-direction measured at the center point of the wafer is shown in Fig. 1, along with the parametric model (5).

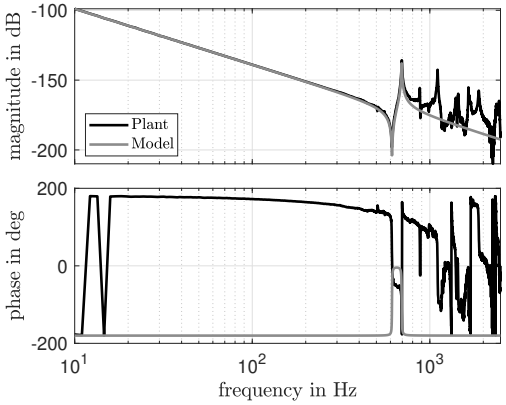

Fig. 1. Measured FRF of the wafer stage in z-direction (black) and simplified fourth-order model (grey).

The simplified motion control scheme of a short-stroke wafer stage in vertical direction is depicted in Fig. 2.

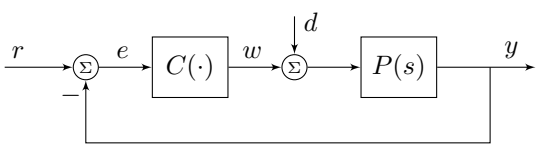

Fig. 2. Simplified closed-loop system configuration.

The input to the stage consists of the control signal w, generated by a (non)linear feedback controller C, and a disturbance d. Dominant sources of (low-frequency) disturbances typically arise from unavoidable cross-talk via hoses, electrical cables, and airshowers used to condition the interferometer measurement system. The plant output

y is subtracted from the reference r to form the servo error signal $e := r - y$. In the remainder, it is assumed that tracking is dealt with by an advanced feedforward controller, and a mismatch in feedforward is regarded as an additional setpoint-induced input disturbance.

3.2 HIGS-Based PID Controller

Consider the following linear PID-type controller structure that is commonly used (after rigid-body decoupling) for wafer stage feedback control:

$$C(s) = C_{pid}(s)C_{lp}(s)C_n(s), \tag{6}$$

where the PID-filter $C_{pid}(s)$ and the second-order low-pass filter $C_{lp}(s)$ are given by

$$C_{pid}(s) = k_p\left(1 + \frac{\omega_i}{s} + \frac{s}{\omega_d}\right), \tag{7}$$

$$C_{lp}(s) = \frac{\omega_{lp}^2}{s^2 + 2\beta_{lp}\omega_{lp}s + \omega_{lp}^2}, \tag{8}$$

with proportional gain $k_p \in \mathbb{R}$, integrator, differentiator, and low-pass cut-off frequencies $\omega_i, \omega_d, \omega_{lp} \in \mathbb{R}$, respectively, and damping coefficient $\beta_{lp} \in \mathbb{R}$. In (6), $C_n(s)$ consists of several notch-filters, *i.e.*,

$$C_n(s) = \prod_{i=1}^{N}\left(\frac{\omega_{p,i}^2}{\omega_{z,i}^2}\right)\frac{s^2 + 2\beta_{z,i}\omega_{z,i}s + \omega_{z,i}^2}{s^2 + 2\beta_{p,i}\omega_{p,i}s + \omega_{p,i}^2}. \tag{9}$$

Although the integrator in (7) and the low-pass filter (8) are key elements for attaining sufficient input disturbance rejection and noise attenuation of the controlled system (Skogestad & Postlethwaite, 2005), these also introduce the negative effects of phase lag. To improve upon this aspect, one may consider replacing these linear filters by HIGS-based equivalent filters. The latter possess similar magnitude characteristics as the filter they intend to replace, but induce significantly less phase lag as observed from their describing functions.

A particular approach for constructing such filters, is through the use of input-output filters. That is, by augmenting the HIGS with linear weighting filters $Z(s), U(s) \in \mathbb{C}$ as demonstrated in Fig. 3, one obtains a cascaded filter element, denoted by H_F, for which the describing function is derived on the basis of linear reasoning as

$$\mathcal{D}_F(j\omega) = Z(j\omega)\mathcal{D}(j\omega)U(j\omega), \tag{10}$$

with $\mathcal{D}(j\omega)$ the HIGS' describing function (4).

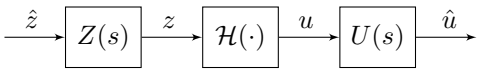

Fig. 3. Augmented HIGS-based filter H_F.

Clearly, $Z(s)$ and $U(s)$ can be exploited for shaping the characteristics of (10). As is motivated in Van den Eijnden et al. (2020), the particular choice

$$Z(s)U(s) = \left(1 + \frac{s}{\omega_c}\right)F(s), \tag{11}$$

where $\omega_c = \omega_h|1 + 4j/\pi|/k_h$ corresponds to the cross-over frequency of (4) and $F(s)$ is the filter whose phase properties are to be improved, *e.g.*, $F(s) = \omega_i/s$ or $F(s) = C_{lp}(s)$, yields the overall describing function (10) to have similar magnitude characteristics as $F(s)$, but with different phase lag. Note that different choices for $Z(s), U(s)$ that satisfy (11) are possible. The rationale for the choice in (11) comes from the fact that $\mathcal{D}(j\omega)$ has magnitude characteristics corresponding to a first-order low-pass filter, which are compensated by the 'inverted' PD-part in (11). Consequently, one achieves $\|\mathcal{D}_F(j\omega)\| = \|Z(j\omega)\mathcal{D}(j\omega)U(j\omega)\| \approx \|F(j\omega)\|$. Furthermore, the 90 degrees phase lead induced by the PD-filter in (11) together with the smaller phase lag of 38.15 degrees coming from $\mathcal{D}(j\omega)$, results in an overall phase lead contribution to the phase characteristics of $\mathcal{D}_F$.

Adopting the use of HIGS-based filters as constructed in Fig. 3 in the PID-based configuration (6), results in the HIGS-based PID controller as depicted in Fig. 4. Here,

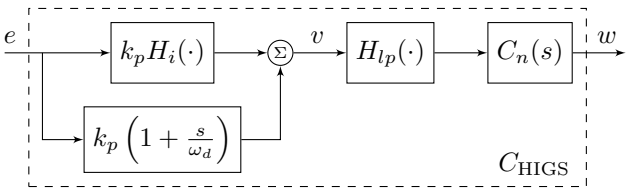

Fig. 4. PID controller, with HIGS-based integrator H_i and HIGS-based second-order low-pass filter H_{lp}.

the HIGS-based integrator H_i is constructed by choosing $Z(s) = 1$ and $U(s) = (1 + s/\omega_c)\,\frac{\omega_i}{s}$, and for the HIGS-based second-order low-pass filter H_{lp}, $Z(s) = 1$ and $U(s) = (1 + s/\omega_c)\,C_{lp}(s)$, with $C_{lp}(s)$ as in (8), are chosen.

In general, a describing function of the HIGS-based PID controller in Fig. 4 cannot be constructed by simply appending the describing functions of the HIGS-based integrator and HIGS-based low-pass filter, as the input to the second HIGS associated with H_{lp} is not necessarily sinusoidal. However, as discussed in Van den Eijnden et al. (2020), if the parameters associated with the two HIGS elements are chosen as to satisfy $\omega_{h,i} < \gamma\omega_{h,lp}$, with $\gamma > 1$ sufficiently large, interference of both nonlinear elements remains fairly limited, and the HIGS-based controller admits a frequency-domain approximation given by

$$\mathcal{D}_C(j\omega) = k_p\left(1 + \mathcal{D}_i(j\omega) + \frac{j\omega}{\omega_d}\right)\mathcal{D}_{lp}(j\omega)C_n(j\omega), \tag{12}$$

in which $\mathcal{D}_i(j\omega)$ and $\mathcal{D}_{lp}(j\omega)$ are the describing functions of the HIGS-based integrator, and second-order low-pass filter, given by (10). The describing function (12) is shown in Fig. 5, together with a linear equivalent PID-controller.

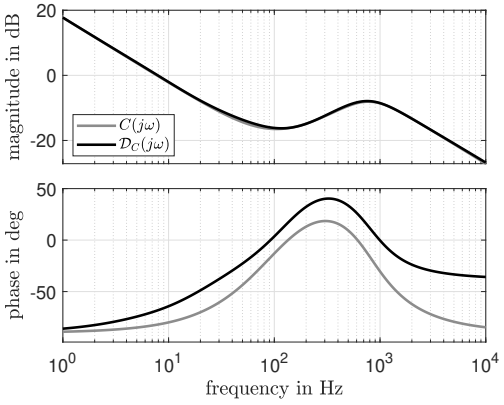

Fig. 5. Frequency-domain characterization of a linear PID controller (grey) and HIGS-based controller (black).

In the remainder of the paper, (12) together with the constraint on $\omega_{h,i}$ and $\omega_{h,lp}$ will be used in a quasi-linear loopshaping design procedure of the HIGS-based PID controller for a wafer stage system.

4. CLOSED-LOOP STABILITY ANALYSIS

Though being valuable for design purposes, a describing function analysis does not provide solid conclusions on stability of a system in feedback with the presented HIGS-based controller. To deal with this shortcoming, in this section rigorous conditions for closed-loop stability are formulated in terms of numerically verifiable LMIs. As this requires the need for a state-space formulation of the closed-loop system, the system in Fig. 2 is first re-written into an equivalent Lur'e form, as shown in Fig. 6.

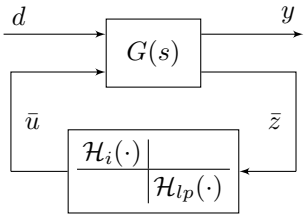

Fig. 6. Closed-loop system in Lur'e form.

Here, $\bar{z} = [z_i, z_{lp}]^\top$ denotes the augmented inputs to the HIGS (1) associated with the integrator and low-pass filter, indicated by the subscripts i, and lp, respectively, and $\bar{u} = [u_i, u_{lp}]^\top$ represents the corresponding outputs. Assume that the multi-input multi-output system $G(s)$ admits the following state-space realization

$$G : \begin{cases} \dot{x}_l &= A_l x_l + B_u \bar{u} + B_l d, \\ y &= C_l x_l + D_u \bar{u} + D_l d, \\ \bar{z} &= C_z x_l + D_z \bar{u}, \end{cases} \tag{13}$$

with states $x_l \in \mathbb{R}^m$, and output $y \in \mathbb{R}$. Note that (13) implies that the transfer from d to $\bar{z}$ is strictly proper, which is the case since $P(s)$ in (5) has a relative degree of two. In turn, this implies $C_z B_l = 0$. The linear system (13) interconnected with two HIGS elements (1) can be written as the following piecewise linear system

$$\begin{aligned} \dot{x} &= A_{pq} x + B d, \quad \text{if } Ex \in \mathcal{F}_{pq}, (p,q) \in \{1,2\}^2 \\ y &= Cx + Dd, \end{aligned} \tag{14}$$

with $x = [x_l, x_{h_i}, x_{h_{lp}}] \in \mathbb{R}^m \times \mathcal{F}_i \times \mathcal{F}_{lp}$, where $\mathcal{F}_i, \mathcal{F}_{lp}$ are the sets associated with $\mathcal{H}_i$ and $\mathcal{H}_{lp}$, respectively, given in (3) and $\mathcal{F}_{pq} = \mathcal{F}_{i,p} \cup \mathcal{F}_{lp,q}$. Note that p indexes the active mode of $\mathcal{H}_i$, whereas q indexes the active mode of $\mathcal{H}_{lp}$, with $p, q = 1$ referring to 'integrator-mode', respectively for $\mathcal{H}_i(\cdot)$ (indicated by p) as well as $\mathcal{H}_{lp}(\cdot)$ (indicated by q), and $p, q = 2$ referring to 'gain-mode'. The matrix E extracts the signals from x that determine mode-switching of the HIGS elements, *i.e.*, $Ex = [E_i, E_{lp}]x = [(z, u, \dot{z})_i, (z, u, \dot{z})_{lp}]^\top$. The system matrices are given by

$$\left[\begin{array}{c|c} A_{pq} & B \\ \hline C & D \end{array}\right] = \left[\begin{array}{cc|c} A_l & B_u & B_l \\ J_{pq}Q_{pq} & J_{pq}R_{pq} & 0 \\ \hline C_l & D_u & D_l \end{array}\right], \tag{15}$$

where the mode dependent matrices are derived as $J_{pq} := (I - K_{pq}D_z)^{-1}$, $Q_{pq} := W_{pq}C_z + K_{pq}C_z A_l$, and $R_{pq} := W_{pq}D_z + K_{pq}C_z B_u$. Furthermore, the matrices

$$W_{pq} := \operatorname{diag}\left([s(p)\omega_{h,i}, s(q)\omega_{h,lp}]\right), \tag{16a}$$

$$K_{pq} := \operatorname{diag}\left([(1-s(p))k_{h,i}, (1-s(q))k_{h,lp}]\right), \tag{16b}$$

select the corresponding active dynamics of each HIGS, with $s(k) := 2 - k$. Note that for deriving the matrices in (15) use is made of the representation $\dot{\bar{u}} = W_{pq}\bar{z} + K_{pq}\dot{\bar{z}}$ with $\bar{u} = \left[x_{h_i}, x_{h_{lp}}\right]^\top$. Moreover, for the considered configuration, the matrix $(I - K_{pq}D_z) \in \mathbb{R}^{2\times 2}$ is invertible.

4.1 LMI-based stability conditions

For reducing possible conservatism in the stability analysis, knowledge about the switching regions of HIGS in (3) can be incorporated in the search for a suitable Lyapunov function via the use of S-procedure relaxation terms. For a general HIGS in (1), these terms are constructed as follows. In integrator mode, the input-output relation is confined to $(k_h z(t))^2 \geq k_h z(t) u(t) \geq u(t)^2$. Using the fact that in a closed-loop system one has $Ex = [z, u, \dot{z}]^\top$, these quadratic inequalities can be written in terms of the state x as

$$x^\top \underbrace{E^\top Q_1 E}_{:=\mathcal{S}_1} x \geq 0, \text{ with } Q_1 = \begin{bmatrix} k_h^2 & k_h & 0 \\ k_h & -2 & 0 \\ 0 & 0 & 0 \end{bmatrix}. \tag{17}$$

Additionally, for the gain mode one has $u(t) = k_h z(t)$, and $\omega_h z(t)^2 - k_h \dot{z}(t) z(t) \geq 0$. The inequality is written as

$$x^\top \underbrace{E^\top Q_2 E}_{:=\mathcal{S}_2} x \geq 0, \text{ with } Q_2 = \begin{bmatrix} 0 & 0 & -k_h \\ 0 & 0 & 0 \\ -k_h & 0 & 2\omega_h \end{bmatrix}, \tag{18}$$

and the equality is captured by $x^\top E^\top \Pi^\top \Pi E x := x^\top \mathcal{T} x = 0$, with $\Pi = [k_h, -1, 0]$. The next theorem presents sufficient conditions for stability of the closed-loop system (14).

Theorem 1. Consider the closed-loop system in (14) with $\|d\|_\infty \leq c$. Suppose there exist non-negative real scalars $\alpha_{xx}, \beta_{pq,xx} \geq 0$, and arbitrary real scalars $\gamma_{pq,xx}$, with $xx = \{i, lp\}$ such that for all $(p,q) \in N^2$, $N = \{1,2\}$, the symmetric matrix $\mathcal{P} \in \mathbb{S}^{n\times n}$ satisfies the following LMIs

$$\mathcal{P} - \Sigma \succ 0, \tag{19a}$$

$$A_{pq}^\top \mathcal{P} + \mathcal{P} A_{pq} + \Theta_{pq} + \Psi_{pq} \prec 0, \tag{19b}$$

where $\Sigma = \alpha_i \mathcal{S}_{1,i} + \alpha_{lp} \mathcal{S}_{1,lp}$, and $\Theta_{pq} = \beta_{pq,i}\Theta_{p,i} + \beta_{pq,lp}\Theta_{q,lp}$ with

$$\Theta_{k,xx} = s(k)\mathcal{S}_{1,xx} + (1 - s(k))\mathcal{S}_{2,xx}, \tag{20}$$

and

$$\Psi_{pq} = \gamma_{pq,i}(1 - s(p))\mathcal{T}_i + \gamma_{pq,i}(1 - s(q))\mathcal{T}_{lp}, \tag{21}$$

with selection function $s(k) = 2 - k$, and where $\mathcal{S}_{k,xx}, \mathcal{T}_{xx}$ are defined in (17) and (18). Then for all $x(0) \in \mathbb{R}^m \times \mathcal{F}_i \times \mathcal{F}_{lp}$ the closed-loop system is input-to-state stable (ISS).

The proof of Theorem 1 demonstrates that under the hypothesis of the theorem, the function $V(x) = x^\top \mathcal{P} x$ qualifies as an ISS Lyapunov function for the system. It is a fairly standard proof (see *e.g.*, Johansson (2003); Khalil (2002)) and is therefore omitted from the paper. Note, however, that key in proving the theorem is the use of the S-procedure (related to the matrices Σ, and Θ_{pq}) and Finsler's lemma (related to Ψ_{pq}), along with the fact that the input d enters linearly in the dynamics (14).

5. LOOPSHAPING DESIGN AND WAFER STAGE MEASUREMENT RESULTS

In this section, two controllers are designed for the wafer stage system in Fig. 2: (i) linear controller $C = C_{\text{lin}}(s)$

with similar structure as in (6), and four fixed notch-filters, and (ii) HIGS-based controller $C = C_{\text{HIGS}}$, as presented in Fig. 4, where $C_n(s)$ consists of four notch-filters that are identical to those used in the linear case. The design procedure employs an automated (quasi-)linear H_∞-loopshaping approach which is formulated as the following generalized constrained optimization problem

$$\begin{aligned} \underset{\rho}{\text{maximize}} \quad & \omega_{bw}(\rho) \\ \text{subject to} \quad & \|W(j\omega)M(j\omega,\rho)\|_\infty \leq 1, \quad \forall \omega \in \Omega, \\ & \rho \in \{\underline{\rho}, \overline{\rho}\}, \end{aligned} \tag{22}$$

where $\rho \in \mathbb{R}^n$ is the set of controller design parameters with $\underline{\rho}, \overline{\rho}$ being the minimum and maximum admissible values, ω_{bw} is the bandwidth to be maximized, and

$$M(j\omega,\rho) = \left(\begin{array}{c|c} S & -PS \\ \hline CS & -CPS \end{array}\right) \in \mathbb{C}^{2\times 2}, \tag{23}$$

is the four block transfer function matrix relating the exogenous inputs r, d to the performance outputs e, w. Here, $P(j\omega)$ is the *measured* plant FRF, see Fig. 1, and $C(j\omega)$ denotes the (quasi-linear) FRF representation of the controller. That is $C(j\omega) = C_{\text{lin}}(j\omega)$ for the linear case whereas $C(j\omega) = \mathcal{D}_C(j\omega)$, with $\mathcal{D}_C(j\omega)$ given in (12) for the HIGS case. The (quasi-linear) sensitivity transfer function is defined by $S(j\omega) = (1 + C(j\omega)P(j\omega))^{-1}$. In (22), $W(j\omega) \in \mathbb{C}^{2\times 2}$ is a dynamic weighting filter that is related to the design criteria (*e.g.*, sensitivity peaking), and $\Omega = \{\omega \in \mathbb{R} \mid \omega_{min} \leq \omega \leq \omega_{max}\}$ is a compact set which contains the frequencies of interest. The optimization problem (22) for both the linear and quasi-linear case is solved by means of an autotuner. The obtained set of parameters are given in Table 1 and Table 2, and the sensitivity magnitude characteristics are shown in Fig. 7.

Table 1. PID-filter parameter values.

	Linear	HIGS	
k_p	$1.51 \cdot 10^7$	$1.94 \cdot 10^7$	N/m
ω_i	$57.99 \cdot 2\pi$	$72.91 \cdot 2\pi$	rad/s
ω_d	$86.99 \cdot 2\pi$	$109.4 \cdot 2\pi$	rad/s
ω_{lp}	$552.5 \cdot 2\pi$	$537.2 \cdot 2\pi$	rad/s
β	0.2	0.2	-
$k_{h,i}$	–	1	-
$\omega_{h,i}$	–	$76.59 \cdot 2\pi$	rad/s
$k_{h,lp}$	–	1	-
$\omega_{h,lp}$	–	$268.6 \cdot 2\pi$	rad/s

Table 2. Notch filter parameter values.

i	$\omega_{z,i}$ in rad/s	$\beta_{z,i}$	$\omega_{p,i}$ in rad/s	$\beta_{p,i}$
1	$740 \cdot 2\pi$	$-1.3 \cdot 10^{-3}$	$620 \cdot 2\pi$	$1.6 \cdot 10^{-1}$
2	$1039 \cdot 2\pi$	1.3	$668 \cdot 2\pi$	1.97
3	$157 \cdot 2\pi$	$2.4 \cdot 10^{-2}$	$160 \cdot 2\pi$	$2.0 \cdot 10^{-2}$
4	$1884 \cdot 2\pi$	$2.4 \cdot 10^{-1}$	$1944 \cdot 2\pi$	$2.0 \cdot 10^{-1}$

Under the given design constraints, the maximum bandwidth obtained with the linear controller is 142 Hz whereas the use of $\mathcal{D}_C(j\omega)$ allows for a somewhat larger bandwidth of 153 Hz. The (quasi-linearized) HIGS-based controller gives rise to a substantial 4.2 dB improvement in broadband low-frequency disturbance suppression as compared to the linear design. This is effectuated by the HIGS-based low-pass filter which induces less phase lag around the bandwidth and thus allows for a larger loop-gain (see Table 1). In the range from 70 Hz to 120 Hz the improvement is even 6.5 dB, which stems from the phase characteristics associated with the HIGS-based integrator H_i.

Remark 1. Verifying stability of the resulting closed-loop system by finding a feasible solution to the LMIs in Theorem 1 appeared to be no trivial task. By increasing $\omega_{h,lp}$ by a factor of at least 1.82, feasible solutions were found. Note that this is remarkable since the conditions in Theorem 1 are possibly conservative due to the search for a *common* quadratic Lyapunov function. The conditions may be further relaxed by considering, *e.g.*, *piecewise* quadratic functions instead (Johansson, 2003). For systems with a single HIGS, such an approach has been succesfully applied in Van den Eijnden et al. (2019).

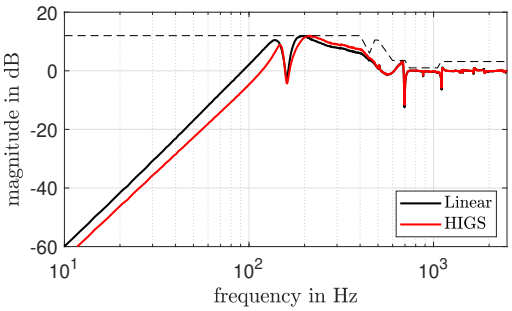

Fig. 7. Sensitivity magnitude characteristics of the linear system and HIGS controlled system along with the sensitivity constraint (dashed).

5.1 Measurement Results

During experiments, the system is subject to a representative third-order scanning setpoint, and a sampling frequency of 5 kHz is used. To quantify servo performance of a wafer scanner, two key performance measures are considered: (i) the moving average (MA) filtered error, and (ii) the moving standard deviation (MSD) filtered error. The MA characterizes the ability of exposing two layers exactly on top of each other (overlay), and is defined as

$$\text{MA}\{e(t)\} := \frac{1}{T_e}\int_{t-\frac{T_e}{2}}^{t+\frac{T_e}{2}} e(\tau)d\tau, \tag{24}$$

with T_e the exposure time. Essentially, (24) resembles a low-pass filtering type of operation applied to the measured error signal e. The MSD provides a measure for imaging quality. It is defined by

$$\text{MSD}\{e(t)\} := \sqrt{\frac{1}{T_e}\int_{t-\frac{T_e}{2}}^{t+\frac{T_e}{2}} \left(e(\tau) - \mathcal{M}_A\{e(\tau)\}\right)^2 d\tau}, \tag{25}$$

and resembles a high-pass filtering operation. The raw error signal e measured at the center point of the wafer, MA, and MSD of eight consecutive experiments for the linear- and HIGS-based configuration are shown in Fig. 8.

First, it is noted form Fig. 8 that the achieved performance over all eight repeated experiments is quite reproducible. Clear improvements in MA and MSD are observed from Fig. 8 for the HIGS-controlled system. Particularly, the

peak values of the MA during the scanning phase decrease from 8.3 nm in the linear case to 4.3 nm for the HIGS controlled case, thereby demonstrating almost a factor of two improvement, which is in agreement with the expectation coming from the describing function in Fig. 7. This sort of improvement is also observed for the MSD values. Note that simultaneous improvements in both MA and MSD is in general not trivial due to (i) the waterbed effect which is associated with linear systems but may still be present in the nonlinear case, (ii) generation of non-smooth control signals which potentially induces more high-frequency distortion, and (iii) the introduction of multiple nonlinearities in the feedback control loop.

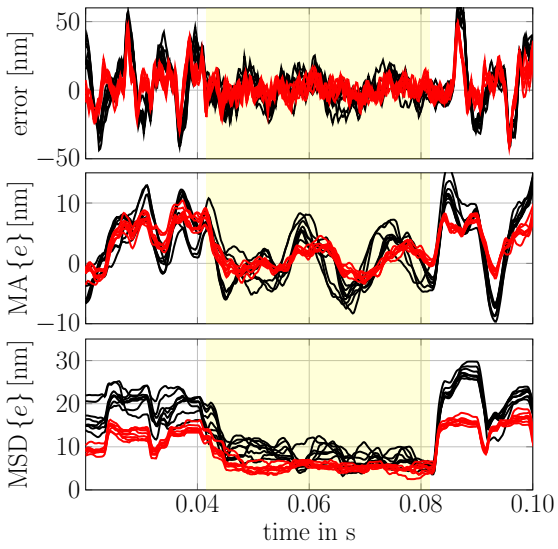

Fig. 8. Error $e(t)$ (top), MA (middle), and MSD (bottom) for the linear (black) and HIGS-controlled system (red). The yellow surface indicates a scanning phase.

In addition to time-domain results, frequency-domain results are presented in Fig. 9 in terms of an averaged cumulative power spectral density (cPSD). From Fig. 9 a significant improvement in mid-frequency disturbance rejection is observed, particularly in the range from 60 – 300 Hz. Also note that around 200 Hz, the linear system induces relatively more amplification than the HIGS controlled system, whereas in the range 400 – 700 Hz, the opposite is observed. These observations are in agreement with the predictions coming from the describing function in Fig. 7, hence its usefulness for motion control design.

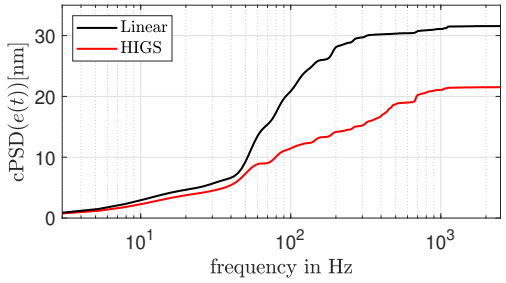

Fig. 9. Cumulative power spectral density of the measured error signal $e(t)$.

6. CONCLUSIONS

In this paper, the use of multiple hybrid integrator-gain elements in a PID-based controller configuration is considered. The reduced phase characteristics associated with these elements are exploited in a describing function based controller design procedure to achieve improved low-frequency disturbance rejection properties when compared to a linear design. Sufficient conditions for stability of the true nonlinear closed-loop system are given in the form of numerically tractable LMIs. Measurement results on a short-stroke wafer stage of an industrial wafer scanner support the potential for improving low-frequency disturbance rejection without excessive transmission of high-frequency noise. Combined use of multiple HIGS elements is therefore believed to significantly contribute to the performance enhancement of industrial high-precision motion systems.

REFERENCES

H. Butler (2011). Position control in lithographic equipment: an enabler for current-day chip manufacturing, *Control Systems, IEEE*, 31(5), pp. 28-47.

M.M. Seron, J.H. Braslavsky, and G.C. Goodwin (1997). Fundamental Limitations in filtering and control. Berlin: Springer.

W. Foster, D. Gieseking, W. Waymeyer (1966). A Nonlinear Filter for Independent Gain and Phase (With Applications), *Trans. of the ASME Journal of Basic Engineering*, 78, pp. 457–462.

O. Beker, C.V. Hollot, Y. Chait, H. Han (2004). Fundamental properties of reset control systems. *Automatica*, 40, pp. 905-915.

D. Nešić, L. Zaccarian, A.R. Teel (2008). Stability properties of reset systems. *Automatica*, 44, pp. 2019-2026.

M.F. Heertjes, N.I. Perdiguero, D.A. Deenen (2018). Robust data-driven tuning of a hybrid integrator-gain system with applications to wafer scanners, *Int. Jour. of Adaptive Control and Signal Process*, 33(2), pp. 371-387.

T.A.E. Oomen, R. van Herpen, S. Quist, M.M.J. van de Wal, O.H. Bosgra, M. Steinbuch (2014). Connecting system identification and robust control for next-generation motion control of a wafer stage, *IEEE Trans. on Control Systems Technology*, 22(1), pp. 102-118.

S.J.A.M. van den Eijnden, M.F. Heertjes, H. Nijmeijer (2020). Experimental Demonstration of a Nonlinear PID-Based Control Design Using Multiple Hybrid Integrator-Gain Elements. *American Control Conference*.

S. Skogestad, I. Postlethwaite (2005). Multivariable feedback control: analysis and design, second edition. Wiley, Chichester, West Sussex, England.

N. Saikumar, R. K. Sinha, S. H. HosseinNia (2019). 'Constant in Gain Lead in Phase' Element – Application in Precision Motion Control, *IEEE/ASME Transactions on Mechatronics*, 24(3), pp. 1176-1185.

M. Johansson (2003). Piecewise Linear Control Systems: A Computational Approach. Springer, Berlin Heidelberg.

H.K. Khalil (2002). Nonlinear Systems. Prentice Hall, Upper Saddle River, New Jersey.

S.J.A.M. van den Eijnden, M.F. Heertjes, H. Nijmeijer (2019). Robust Stability and Nonlinear Loop-Shaping Design for Hybrid Integrator-Gain-Based Control Systems. *American Control Conference*, pp. 3063-3068.